Fast computation of multivariate synchrony index in sliding windows: application to cardiac neurons

Jean-Philippe Longpré[1,2], Siamak Salavatian[1,2], Eric Beaumont[3], J. Andrew Armour[4], Jeffrey L. Ardell[4], Vincent Jacquemet[1,2]

[1] Centre de Recherche, Hôpital du Sacré-Coeur de Montréal, 5400 boul. Gouin Ouest, Montréal (Québec) H4J 1C5, Canada.
[2] Department of Physiology, Université de Montréal, Montr eal, QC, Canada.
[3] Department of Biomedical Sciences, East Tennessee State University, Johnson City, TN, USA.
[4] Cardiac Arrhythmia Center, UCLA, Los Angeles, CA, USA.

September 2014

E-mail: vincent.jacquemet@umontreal.ca

Abstract. Multielectrode array neuronal recordings in atrial ganglionated plexi are characterized by low firing rates, marked non-stationarity, interplay with the cardiovascular and pulmonary systems and artifacts generated by myocardial activity, which creates challenges very different from brain recordings. To explore population dynamics of intrinsic cardiac neurons, a jitter-based synchrony index has been defined to quantify pairwise synchrony between neurons. In this paper, we extend this synchrony index to multiple time series in order to monitor global (multivariate) synchrony. Numerical techniques are developed to efficiently compute synchrony indices and their statistical significance in a large number of time windows. A scale-time graphical representation is proposed to visualize synchrony in sliding windows of varying lengths. This approach is validated in synthetic time series and in experimental data sets recorded in 11 dogs. Results show the ability of the method to monitor synchrony over time in neuron populations, between neurons and the cardiopulmonary system and between neuron firing and electrical stimulation. These tools will facilitate the exploration and robust quantitative analysis of multiple-hour recordings in cardiac ganglionated plexi to efficiently identify relevant periods of activity in relation to physiological or external stimuli and cardiac arrhythmia.

1. Introduction

The heart receives sympathetic and parasympathetic efferent innervation via the intrinsic cardiac nervous system in order to regulate its electrical and mechanical activity (Armour et al. 1994, Ardell 2004). Populations of cardiac neurons in atrial and ventricular ganglionated plexi receive inputs from central neurons and from mechano- and chemoreceptors located in the heart and adjacent vessels (Armour and Kember 2004). Local circuit neurons are hypothesized to form a local processor of information, the "little brain in the heart" (Armour 2007, Armour 2008), that coordinate regional cardiac indices under the influence of efferent central neurons. The structure and function of this network, however, remain largely unknown.

To study this neural network, electrophysiological recordings in ganglionated plexi can be performed by inserting an electrode in the nervous tissue. Linear multielectrode array technology enabled simultaneous recording of a small population of cardiac neurons (5 to 28) in canine right atrium ganglionated plexi for multiple hours (Beaumont et al. 2013). These data opened the way to new investigation about the organization of these neurons and their interactions with the cardiovascular system, but also created signal analysis challenges.

In a previous study, we adapted the synchrony index (SI) developed in Agmon (2012) to quantify the synchrony between pairs of cardiac neurons and between neurons and the cardiovascular and pulmonary systems (Longpré et al. 2014). This SI is well-normalized, independent of variations in firing rate and relies on analytical formulas so that its statistical significance can be assessed without explicit generation of numerous surrogate spike trains. Such properties are required in the context of cardiac neurons because their firing rates are relatively low (0.1 to 5 Hz typically) and highly non-stationary, notably due to the modulation by the cardiovascular and pulmonary systems. Owing to low firing rates, synchrony among cardiac neurons could possibly be small, so its quantification needs to remain applicable and sensitive at low values.

The aim of this paper is to extend this work to create a multivariate synchrony index (MSI) amenable to fast computations for a large number of time windows. This is important for the following reasons. Due to highly non-stationary activity, synchrony is expected to vary along time, possibly switching between periods of insignificant synchrony and periods of synchronized activity. To identify and characterize these periods, sliding windows of varying durations may be used. Since the analysis needs to be carried out in many time intervals, computational efficiency becomes critical. By pooling the data from multiple neurons together, a MSI may facilitate the identification of these periods of synchronized activity and provide a single symmetric measure of the synchrony of a group of neurons. Further analysis may then be performed on a pair or a subset of neurons.

Several techniques for measuring the synchrony of central neuron populations have been developed, as reviewed in Pereda et al. (2005). A straightforward multivariate technique consists in taking the average of pairwise synchrony (Kreuz et al. 2009, Kreuz

et al. 2013). Another approach is to create a model of the multivariate point process representing neuron firing, for instance using multinomial generalized linear models (Ba et al. 2014), multivariate autoregressive models (Ba et al. 2014), directed transfer function (Kaminski and Blinowska 1991) or gravity transform (Lindsey and Gerstein 2006). Model-based methods are however sensitive to parameter estimation which requires enough data to be accurate. Some measures use a cumulative spike train obtained by pooling all the different spike trains together (Hunter et al. 1998, Tiesinga 2004). Another multivariate measure may be obtained by computing the coefficient of variation of the interspike intervals (Kreuz et al. 2009). Gersch and Goddard (1970) used partial coherence that takes into account a third time series to correct the estimation of the coherence of two time series. There is some debate on the reliability of this technique relative to noise contamination (Albo et al. 2004, Baccala and Sameshima 2006). Allefeld and Kurths (2004) developed a measure based on phase synchronization of an ensemble of different oscillators (recording sites) relative to the phase of a statistical cluster, the later being defined as a weighted mean of the phase of the individual oscillators.

While these methods provide valuable insight into multivariate synchrony, they require the use of surrogate data to assess if synchrony is statistically significant. To bypass this shortcoming, we propose to create a multivariate extension of the SI that was described in Longpré et al. (2014). In addition, to deal with sparsely distributed neuronal activity inherent to cardiac neurons, we devised a window analysis tool able to rapidly and systematically search a whole recording for intervals of various durations where multivariate synchrony is measurable and statistically significant.

This article is organized as follows. The definition of the SI and MSI measures and their calculation in sliding windows are first described. A methodology to generate synthetic data characterized by a given MSI is introduced. Then, synthetic and experimental time series are used to illustrate the applications of our approach to compute the SI between cardiac neurons and physiological signals and the MSI among cardiac neurons.

2. Material and methods

2.1. Synchrony index

In the framework of Agmon's approach, neuron synchronization is analyzed by pair of neurons (Agmon 2012). Since the synchrony index is not symmetric, one neuron is considered the reference and the other one the target. During the interval of analysis, the reference neuron fires at times $\mathbf{t}^1 = (t_1^1, \ldots, t_{n_1}^1)$ and the target neuron at times $\mathbf{t}^2 = (t_1^2, \ldots, t_{n_2}^2)$.

Coincidence is defined as the reference and target neurons both firing within a time window of duration τ_s. For each spike i of the reference neuron, the occurrence of a

coincidence is expressed as the vector $\mathbf{S}(\mathbf{t}^1, \mathbf{t}^2)$ of dimension n_1 whose entries are:

$$S_i = \begin{cases} 1 & \text{if} \quad t_i^1 \in \bigcup_{j=1}^{n_2} [t_j^2 - \tau_s, t_j^2 + \tau_s] \\ 0 & \text{otherwise} \end{cases} \tag{1}$$

The number of coincidences N_c can be computed as the scalar product:

$$N_c(\mathbf{t}^1, \mathbf{t}^2) = \mathbf{S}(\mathbf{t}^1, \mathbf{t}^2) \cdot \mathbf{1}_{n_1} \tag{2}$$

where $\mathbf{1}_n$ is the vector of dimension n with all components set to 1. Some of these coincidences may occur by pure chance. These random coincidences are identified by counting those remaining after random jitter of the spikes of the reference neuron within time windows of duration $2\tau_J$, with the constraint $\tau_J > \tau_s$ (Agmon 2012). If the firing time of the i-th spike of the reference neuron is uniformly distributed in the interval $[t_i^1 - \tau_J, t_i^1 + \tau_J]$, the probability of coincidence is given by the vector $\mathbf{p}(\mathbf{t}^1, \mathbf{t}^2)$ of dimension n_1 whose entries are

$$p_i = \frac{1}{2\tau_J}\ \mu\left([t_i^1 - \tau_J, t_i^1 + \tau_J]\ \cap\ \bigcup_{j=1}^{n_2} [t_j^2 - \tau_s, t_j^2 + \tau_s] \right) \tag{3}$$

where $\mu(W)$ is the measure (total length) of the set W.

The occurrence S_i^J of coincidence after jitter is a Bernoulli random variable with mean p_i. The number of random coincidences is $N_c^J = \sum_{i=1}^{n_1} S_i^J$. Since the random variables S_i^J are independent, the mean $\langle N_c^J \rangle = \sum_{i=1}^{n_1} p_i$ and variance $\sigma_J^2 = \sum_{i=1}^{n_1} p_i(1 - p_i)$ of N_c^J can be expressed as:

$$\langle N_c^J \rangle(\mathbf{t}^1, \mathbf{t}^2) = \mathbf{p} \cdot \mathbf{1}_{n_1} \tag{4}$$

$$\sigma_J^2(\mathbf{t}^1, \mathbf{t}^2) \quad = \mathbf{v} \cdot \mathbf{1}_{n_1} \tag{5}$$

where the components of $\mathbf{v}(\mathbf{t}^1, \mathbf{t}^2)$ are $v_i = p_i(1 - p_i)$. Agmon's synchrony index SI is defined as

$$SI(\mathbf{t}^1, \mathbf{t}^2) = \beta\ \frac{N_c - \langle N_c^J \rangle}{n_1} \tag{6}$$

where $\beta = \tau_J/(\tau_J - \tau_s)$ if $\tau_J \geq 2\tau_s$ and $\beta = 2$ otherwise.

To test the hypothesis that the synchrony is not due to chance, the observed coincidence count is compared to the distribution of random coincidences. The p-value is defined as the probability that $N_c^J > N_c$ when $SI > 0$ and the probability that $N_c^J < N_c$ when $SI < 0$. The distribution is approximately normal so the p-value is related to the Z-score (Agmon 2012):

$$Z(\mathbf{t}^1, \mathbf{t}^2) = \frac{N_c - \langle N_c^J \rangle}{\sigma_J} = \frac{n_1 SI}{\beta \sigma_J}\ . \tag{7}$$

2.2. Multivariate synchrony index

Suppose we have m neurons with firing time series $\mathbf{t}^k$ of size n_k for $k = 1, \ldots, m$. The total number of spikes $n_1 + \cdots + n_m$ is denoted by n_{tot}. The time series $\tilde{\mathbf{t}}^k$ is defined as the combination of the spikes of all neurons other than k, i.e. the concatenation $\tilde{\mathbf{t}}^k = [\mathbf{t}^1; \ldots; \mathbf{t}^{k-1}; \mathbf{t}^{k+1}; \ldots; \mathbf{t}^m]$ whose size is $n_{tot} - n_k$. For better computational efficiency, the vector $\tilde{\mathbf{t}}^k$ is sorted.

We propose that the multivariate synchrony index (MSI) is defined as:

$$MSI(\mathbf{t}^1, \ldots, \mathbf{t}^m) = \sum_{k=1}^{m} \frac{n_k}{n_{tot}} \, SI\left(\mathbf{t}^k, \tilde{\mathbf{t}}^k\right) \tag{8}$$

$$= \frac{\beta}{n_{tot}} \sum_{k=1}^{m} \left(\mathbf{S}(\mathbf{t}^k, \tilde{\mathbf{t}}^k) - \mathbf{p}(\mathbf{t}^k, \tilde{\mathbf{t}}^k)\right) \cdot \mathbf{1}_{n_k} \; . \tag{9}$$

This definition is symmetric with respect to any permutation of the variables $\mathbf{t}^1, \ldots, \mathbf{t}^m$, and the constraint $-2 \leq SI \leq 1$ also applies to MSI. This equation can be rewritten as

$$MSI(\mathbf{t}^1, \ldots, \mathbf{t}^m) = \beta \, \frac{N_c^{tot} - \langle N_c^J \rangle^{tot}}{n_{tot}} \tag{10}$$

where $N_c^{tot} = \sum_{k=1}^{m} \mathbf{S}(\mathbf{t}^k, \tilde{\mathbf{t}}^k) \cdot \mathbf{1}_{n_k}$ is the total number of coincidences between all pairs of neurons and $\langle N_c^J \rangle^{tot} = \mathbf{p}(\mathbf{t}^k, \tilde{\mathbf{t}}^k) \cdot \mathbf{1}_{n_k}$ is the corresponding expected number of random coincidences. Note the similarity with (6). The variance of the number of random coincidences is given by

$$\sigma_J^{tot^2}(\mathbf{t}^1, \ldots, \mathbf{t}^m) = \sum_{k=1}^{m} \mathbf{v}(\mathbf{t}^k, \tilde{\mathbf{t}}^k) \cdot \mathbf{1}_{n_k} \; . \tag{11}$$

As a result, the Z-score can be expressed as

$$Z^{tot}(\mathbf{t}^1, \ldots, \mathbf{t}^m) = \frac{n_{tot} \, MSI(\mathbf{t}^1, \ldots, \mathbf{t}^m)}{\beta \, \sigma_J^{tot}(\mathbf{t}^1, \ldots, \mathbf{t}^m)} \; . \tag{12}$$

2.3. Synchrony index in a time window

To compute the synchrony index $SI(\mathbf{t}^1, \mathbf{t}^2; a, b)$ of neuronal activity within a given time window $]a, b]$, only the terms involving spikes at time $t_i^k \in]a, b]$ are included. The synchrony index can be expressed using the vector function $\mathbf{I}(\mathbf{t}; a, b)$ with the same size as $\mathbf{t}$ defined by $I_i(\mathbf{t}; a, b) = 1$ if $t_i \in]a, b]$ and 0 otherwise. Using this notation,

$$SI(\mathbf{t}^1, \mathbf{t}^2; a, b) = \frac{\beta}{n_1}\left(\mathbf{S}(\mathbf{t}^1, \mathbf{t}^2) - \mathbf{p}(\mathbf{t}^1, \mathbf{t}^2)\right) \cdot \mathbf{I}(\mathbf{t}^1; a, b) \tag{13}$$

$$\sigma_J^2(\mathbf{t}^1, \mathbf{t}^2; a, b) = \mathbf{v} \cdot \mathbf{I}(\mathbf{t}^1; a, b) \; . \tag{14}$$

Once the vectors $\mathbf{S}$, $\mathbf{p}$ and $\mathbf{v}$ are determined for the whole recording, the synchrony index can be easily computed in time windows from expressions of the form $f(a, b; \mathbf{t}, \mathbf{w}) = \mathbf{w} \cdot \mathbf{I}(\mathbf{t}; a, b)$. In practical applications with sliding windows, we would like to evaluate

$f(a, b; \mathbf{t}, \mathbf{w})$ for many values of a and b but the same $\mathbf{w}$ and $\mathbf{t}$. The cumulative distribution function

$$F(c; \mathbf{t}, \mathbf{w}) = \sum_{i\,:\,t_i \le c} w_i \tag{15}$$

is a single-variable function of c, for $\mathbf{t}$ and $\mathbf{w}$ fixed, that is constant by intervals with discontinuities at $\{t_i\}$. This function can therefore be evaluated *exactly* based on look-up tables with nearest-neighbor interpolation. Then, the relation $f(a, b; \mathbf{t}, \mathbf{w}) = F(b; \mathbf{t}, \mathbf{w}) - F(a; \mathbf{t}, \mathbf{w})$ is used. This leads to considerable speedup as compared to computing the SI separately in each time window. The same method applies to the computation of the MSI.

2.4. Generation of synthetic time series

The estimation of the synchrony index will be first assessed in synthetic signals. Our aim is to generate in the time interval $[0, T]$ two time series $\mathbf{t}^1$ and $\mathbf{t}^2$ with firing rates f_1 and f_2 such that their synchrony index $SI(\mathbf{t}^1, \mathbf{t}^2)$ has a given positive value SI. The number of spikes in each time series n_1 and n_2 will be given by $f_1 T$ and $f_2 T$, rounded to the nearest integer; SI will be assumed to be of the fractional form $SI = n_c/n_1$ where n_c is an integer smaller than n_2.

The target time series $\mathbf{t}^2$ is generated as a realization of a Poisson process with firing rate f_2 and a refractory period of $2\tau_s$ to prevent successive spikes from being too close to each other (Fig. 1A). To generate the reference time series $\mathbf{t}^1$, note that when a single spike is added at time t to the reference neuron, the synchrony index as a function of t is $SI(t, \mathbf{t}^2)$. This function, shown on Fig. 1B, is piecewise linear with discontinuities in slope or value at $t = t_j^2 \pm \tau_s$ or $t = t_j^2 \pm (\tau_s + \tau_J)$ for all j.

One way to obtain a synchrony index of $SI = n_c/n_1$ is to place n_c spikes in the set $\Omega_1 = \{t \mid SI(t, \mathbf{t}^2) = 1\} = \bigcup_{k=1}^{m_1} [a_k, b_k]$ and $n_1 - n_c$ spikes in the set $\Omega_0 = \{t \mid SI(t, \mathbf{t}^2) = 0\} = \bigcup_{k=1}^{m_0} [c_k, d_k]$. Since the intervals $[a_k, b_k]$ are short (typically of length $2\tau_s$), n_c of the m_1 intervals are randomly selected and spikes are added randomly (uniform distribution in $[a_k, b_k]$) in these selected intervals (Fig. 1C). To place the remaining $n_1 - n_c$ spikes, the intervals $[c_k, d_k]$ are put together to form a unique interval of duration $T_0 = \sum_{k=1}^{m_0} d_k - c_k$. The $n_1 - n_c$ spikes are distributed in the interval $[0, T_0]$ according to a Poisson process with firing rate $(n_1 - n_c)/T_0$ and a refractory period of $2\tau_s$. These spikes are then moved back in their respective interval $[c_k, d_k]$ (Fig. 1C).

For the generated time series $\mathbf{t}^1$ and $\mathbf{t}^2$, the number of coincidences N_c is n_c. By excluding spikes outside $\Omega_0 \cup \Omega_1$, the average number of random coincidences $\langle N_c^J \rangle$ is guaranteed to be zero, so that the synchrony index $SI(\mathbf{t}^1, \mathbf{t}^2)$ is n_c/n_1 as expected. Reciprocally, because of the refractory period in the generation of the Poisson process, $SI(\mathbf{t}^2, \mathbf{t}^1)$ is n_c/n_2. As a result, $MSI(\mathbf{t}^1, \mathbf{t}^2) = 2n_c/(n_1 + n_2)$, which means that two time series $\mathbf{t}^1$ and $\mathbf{t}^2$ with a given multivariate synchrony index of MSI are generated when $n_c = MSI\ (n_1 + n_2)/2$ is used. Note the general constraint

$$MSI \le 2/(1 + \max(n_1, n_2)/\min(n_1, n_2)) \le 1\ . \tag{16}$$

In other words, the MSI cannot be arbitrarily large when the two time series have very different firing rates.

2.5. Experimental data

Eleven mongrel dogs underwent bilateral open chest surgery in a study approved by the Institutional Animal Care and Use Committee of East Tennessee State University and described in detail in (Beaumont et al. 2013). In this protocol, different electrical stressors were applied to elicit a neuronal response in the right atrium ganglionated plexus. The activity generated by neurons located in this ganglionated plexus was recorded for about 5 hours by means of a multichannel microelectrode array (Linear Microelectrode Array, MicroProbes Inc., Guithersberg, MD) *in situ* under anesthesia (α-chloralose) and controlled respiration (using an artificial respirator). This microelectrode array, consisting of 16 platinum/iridium electrodes (25 μm diameter electrode with an exposed tip of 2 mm; impedance 0.3-0.5 MΩ at 1 kHz), was embedded in the fat that contained the ganglionated plexus such that its tip was placed adjacent to right atrial myocardium. In addition, a bipolar electrode was sewn to the atrial myocardium close to the ganglionated plexus to provide a reference atrial electrogram and assist the identification of atrial activity in neuronal recordings. Left ventricular chamber pressure was continuously recorded using a pressure transducer catheter. Respiration cycles were monitored using a gauge pressure sensor in the exit tube of the respirator. The signals were digitized at a sampling frequency of 5.26 kHz (neuronal signals) or 0.877 kHz (other signals) via a Cambridge Electronics Design data acquisition system (model 1401).

Trains of five electrical stimuli (0.3-1.2 mA, 1 ms duration, 5 ms pulse interval) were delivered for up to 20 seconds to selected mediastinal nerve sites during the refractory period of each atrial beat. This stimulation protocol was used to assess vulnerability to neurogenic atrial fibrillation (AF). Electrical stimuli were delivered via a roving bipolar probe electrode (1.5 mm spacing) connected to a constant current generator (PSIU6, Grass Instruments, Quincy, MA) affixed to a Grass S88 stimulator (S88, Grass Instruments, Quincy, MA).

Spike sorting was performed and validated using Spike2 software (Beaumont et al. 2013). Between 3 and 21 different neuronal waveforms were identified in each of the 11 dogs. When supra-threshold activity was *simultaneously* present in >2 channels, the spike was classified as myocardial electrical activity or motion artifact and all channels were blanked in a 26-ms window around that spike. This identification was validated using the right atrium electrogram.

The data used in this paper are: (1) for each neuron, the time series of spike timings; (2) the left ventricular pressure signal; (3) the respiration pressure signal; and (4) the timing ot the mediastinal nerve stimulation pulses.

3. Results

3.1. Multivariate synchrony in synthetic time series

3.1.1. Two neurons. Two synthetic time series $\mathbf{t}^1$ and $\mathbf{t}^2$ of duration 7 min were generated, following the method of sect. 2.4. Their activity was stationary in each of the 7 consecutive one-minute intervals, but their firing rates f_k^1 and f_k^2 and multivariate synchrony index MSI varied according to Table 1. As a result, the activity was characterized by periods of high and low activity and by periods of significant and insignificant synchrony. The coincidence parameters were set to $\tau_J/2 = \tau_s = 40$ ms as in Longpré et al. (2014).

Interval (k)	1	2	3	4	5	6	7
f_k^1, f_k^2 (Hz)	1	1	1	4	1	4	1
$MSI(\mathbf{t}^1, \mathbf{t}^2)$	0	0.3	0	0.3	0	0	0

Table 1. Firing rate and MSI value in each of the 7 intervals of simulated data.

Using $\mathbf{t}^1$ and $\mathbf{t}^2$, total firing rate and MSI were calculated in time windows ranging from 10 to 60 s in length (by steps of 1 s) and centered on each second of simulated data. For this 420 s simulation, total firing rate and MSI were evaluated in $51 \times 421 = 21,471$ windows. Figure 2B and C depict, respectively, the mean total firing rate and the mean MSI resulting from 5,000 realizations of $\mathbf{t}^1$ and $\mathbf{t}^2$.

The spikes in $\mathbf{t}^1$ and $\mathbf{t}^2$ were placed so that $MSI = 0.3$ when calculated in a 60 s window centered at 90 s (interval 2) or 210 s (interval 4). Figure 2C shows that the mean MSI over a sufficient number of realizations of $\mathbf{t}^1$ and $\mathbf{t}^2$ was also 0.3 for shorter windows inside interval 2 (or 4). The mean MSI value decreased when evaluated in a window partially outside interval 2 (or 4) and became zero for windows completely outside the interval. The rate at which MSI decreased as windows progressively moved out of an interval where spikes were synchronized was faster for interval 2 (lower firing rate) than for interval 4 (higher firing rate). For all window sizes, $MSI = 0.15$ when half of a window was inside interval 2, while $MSI = 0.24$ when interval 4 was considered. This was due to the total firing rate being greater in interval 4 (8 Hz) relative to intervals 3 and 5 (2 Hz), but remaining identical in interval 2 and intervals 1 and 3 (2 Hz). The regions delimiting the boundaries between $MSI = 0$ and the first windows where $MSI > 0$ on each side of interval 2 (or 4) can be represented by straight lines with a slope of 2 (left) or -2 (right). The absolute value of this slope is the result of identifying a window timing using its center, so that there is a delay of half a window length when the edge of a window touches the edge of interval 2 (or 4). The earliest window where mean $MSI > 0$ was a 60 s window centered at 31 s. There was then a 25 s period over which $SI > 0$ started to occur in progressively smaller windows until a 10 s window entered interval 2 at 56 s.

3.1.2. Four neurons. Four synthetic time series $\mathbf{t}^1$, $\mathbf{t}^2$, $\mathbf{t}^3$ and $\mathbf{t}^4$ of duration 11 min were generated by applying the method of sect. 2.4 twice (once for $\mathbf{t}^1$, $\mathbf{t}^2$ and, independently, once for $\mathbf{t}^3$, $\mathbf{t}^4$). Their activity was stationary in each of the 11 consecutive one-minute intervals, but their firing rates $f_k^1 = f_k^2$ and $f_k^3 = f_k^4$ and multivariate synchrony index MSI varied according to Table 2. Non-synchronized portions of the time series were generated as a realization of a Poisson process with a refractory period of $2\tau_s$. As a result, the activity was characterized by periods of high and low activity and by periods of significant and insignificant synchrony.

Interval (k)	1	2	3	4	5	6	7	8	9	10	11
f_k^1, f_k^2 (Hz)	1	1	1	4	1	4	1	1	1	1	1
f_k^3, f_k^4 (Hz)	1	1	1	4	1	4	1	1	1	0	1
$MSI(\mathbf{t}^1, \mathbf{t}^2)$	0	0.3	0	0.3	0	0	0	0.3	0	0.3	0
$MSI(\mathbf{t}^3, \mathbf{t}^4)$	0	0.3	0	0.3	0	0	0	0	0	0	0

Table 2. Firing rates and MSI values in each of the 11 intervals of simulated data.

Total firing rate and MSI were calculated in time windows of 10 to 60 s duration. The mean total firing rate and mean MSI resulting from 5,000 realizations of $\mathbf{t}^l$ for $l = 1, 2, 3, 4$ are shown in Fig. 3B and C, respectively.

In interval 2, spikes were placed to obtain $MSI(\mathbf{t}^1, \mathbf{t}^2) = 0.3$ and $MSI(\mathbf{t}^3, \mathbf{t}^4) = 0.3$. When the mean $MSI(\mathbf{t}^1, \mathbf{t}^2, \mathbf{t}^3, \mathbf{t}^4)$ was calculated using all 4 time series, we found $MSI = 0.2575$ for a 60-s window centered at 90 s, and $MSI = 0.2613$ when a 10-s window centered at 65 or 115 s was used. This decrease in MSI reflects the increased number of expected random coincidences that get subtracted when evaluating Eq. (9). The two mean $MSI(\mathbf{t}^1, \mathbf{t}^2, \mathbf{t}^3, \mathbf{t}^4)$ values were halved when the windows were centered on an edge of interval 2, since total firing rates were the same in intervals 1, 2 and 3. Interval 4 also had $MSI(\mathbf{t}^1, \mathbf{t}^2) = MSI(\mathbf{t}^3, \mathbf{t}^4) = 0.3$, but the firing rate of each time series was higher at 4 Hz, as compared to 1 Hz in interval 2. This resulted in a $MSI(\mathbf{t}^1, \mathbf{t}^2, \mathbf{t}^3, \mathbf{t}^4)$ of 0.1291 when evaluated in a 60-s window centered at 210 s. As it was discussed in section 3.1.1, the higher total firing rate in interval 4 relative to intervals 3 and 5 led to a slower decrease in MSI when calculated in windows partially outside the interval. For a 60 s window half outside interval 4, $MSI = 0.103$.

To further investigate the interplay between synchronized and randomly firing neurons, it is interesting to compare interval 2 to intervals 8 and 10, where only one pair of time series was synchronized so that $MSI(\mathbf{t}^1, \mathbf{t}^2) = 0.3$. In interval 8, the randomness added by $\mathbf{t}^3$ and $\mathbf{t}^4$ reduced $MSI(\mathbf{t}^1, \mathbf{t}^2, \mathbf{t}^3, \mathbf{t}^4)$ down to 0.1278 when evaluated in a 60 s window centered at 510 s, a value even lower than what was found in interval 2. MSI values obtained in windows inside interval 8 were halved when the window center was moved to an edge of the interval. In interval 10, no spikes were placed in $\mathbf{t}^3$ and $\mathbf{t}^4$, which made it possible to get $MSI(\mathbf{t}^1, \mathbf{t}^2, \mathbf{t}^3, \mathbf{t}^4) = 0.3$. However, when $MSI(\mathbf{t}^1, \mathbf{t}^2, \mathbf{t}^3, \mathbf{t}^4)$ was calculated in windows partially outside the interval, its value

decreased faster than $MSI(\mathbf{t}^1, \mathbf{t}^2)$, since the contribution of spikes from $\mathbf{t}^3$ and $\mathbf{t}^4$ in intervals 9 and 11 increased the total number of spikes n_{tot} used in Eq. (8) and added random coincidences after jitter. For that reason, $MSI = 0.1$ for windows half outside interval 10.

3.1.3. Computational time. The analysis software was implemented in Matlab, with some critical parts of the code written in C and integrated as mex files. The performance of the sliding windows analysis tool was tested by monitoring the CPU time needed to compute MSI values as a function of the number of windows and the total number of spikes (Table 3). When the number of windows was small, 10^3 or 10^4, an increase in the number of spikes from 10^5 to 10^6 was reflected by a computational time that was 10 or 5 times longer, respectively. This indicates that the calculation of MSI for the total signal was the bottleneck step in this case. When the number of windows was large ($> 10^5$), the number of spikes did not affect the execution time significantly. This suggests that, in this situation, the step limiting the speed of the calculation was the interpolation associated with windowing following the evaluation of the MSI of the whole signal.

The results of Table 3 show that it took approximately 13 s to calculate the MSI in 10^6 time windows when there were 10^6 spikes in the whole signal. The use of parallel computing would provide further speedup. For a small number of windows, CPU time was proportional to the number of spikes (CPU load was dominated by coincidence identifications). For a very large number of windows, CPU time was not very sensitive to the number of spikes (CPU load was dominated by nearest-neighbor interpolations). The number of spikes that were typically found in the experimental data we work with ($< 5 \times 10^4$), as well as the number of windows we used while performing its analysis ($< 10^5$) are considerably smaller than in the example from Table 3, illustrating the efficiency of our method in the context of intrinsic cardiac neurons.

		# spikes	
		10^5	10^6
# windows	10^3	0.05 ± 0.0004 s	0.48 ± 0.003 s
	10^4	0.12 ± 0.0006 s	0.59 ± 0.002 s
	10^5	1.13 ± 0.005 s	1.69 ± 0.008 s
	5×10^5	6.14 ± 0.02 s	6.84 ± 0.02 s
	10^6	12.60 ± 0.03 s	13.37 ± 0.03 s

Table 3. Mean computational time (± standard deviation) in seconds of 100 random realizations as a function of the number of spikes and the number of windows. The number of spikes was equally distributed among 10 neurons. The duration of windows ranged from 10 to 180 s.

3.2. Synchrony between cardiac neurons and physiological signals

3.2.1. Left ventricular pressure (LVP). Figure 4 shows the firing rate of a neuron as well as the SI between that neuron and a time series generated from the timings of the peak value of LVP signal in each cardiac cycle. LVP time series were considered the "target neuron," so that the SI quantifies the fraction of neuron firings that occurred near peaks of LVP. The SI was calculated using a τ_s of 30 ms in windows from 10 to 180 s in duration centered every 10 s of the experiment. There was no clear link between firing rate and SI, but we observed that higher firing rates tended to reduce the SI by adding random coincidences. Annotated AF episodes all corresponded to periods of low SI, suggesting that AF may disturb cardiovascular related neuronal firing. Over the selected 5,000 s interval, $SI > 0.1$ in 72% and $SI > 0.3$ in 18% of the windows where synchrony was statistically significant at the $p < 0.01$ level, suggesting that this neuron received some cardiovascular-related input.

3.2.2. Respiration. The SI between a neuron and the time series constructed from the peaks of the respiration signal is depicted in Fig. 5 in a 12,000-s region where respiration frequency was $0.14 - 0.19$ Hz. SI was calculated using a coincidence window of 1.5 s, as suggested by Longpré et al. (2014), in time windows from 10 to 180 s in duration centered every 10 s of the recording. To estimate the fraction of neuronal firings that took place in the vicinity of respiratory peaks, the respiration time series was treated as the "target neuron". SI was > 0.5 in 98% and $SI = 1$ in 65% of the windows where it was statistically significant ($p < 0.01$), making the reference neuron strongly respiratory related in that period. AF episodes tended to lower the otherwise high SI values between the neuron and respiration, suggesting that AF could influence the activity of respiratory related neurons by feeding additional inputs.

3.2.3. Mediastinal nerve stimulation. Previous studies suggested that most recorded cardiac neurons in ganglionated plexi were local circuit neurons, which made it less likely to observe direct response to nerve stimulation (Beaumont et al. 2013). Computation of SI in sliding windows provides a convenient and time-efficient way to identify direct response to stimulation when they occur. An example of a neuron synchronized with mediastinal nerve stimulation (MNS) times is shown in Fig. 6. The SI was calculated using a τ_s of 30 ms in windows from 10 to 180 s in duration centered every 10 s. To quantify the fraction of neuron spikes that occurred within a coincidence window of MNS timings, MNS was treated as the "target neuron". Statistically significant synchrony occurred during a 18-s long MNS that was unable to induce AF. Considering all windows completely or partially inside that MNS interval, SI values ranged from 0.36 to 0.9. The highest SI value occurred in a 25 s window centered 3 s after the end of the MNS. The straight line with a slope of 2 drawn on Fig. 6C represents the expected slope of the side of the "triangle" of windows when synchrony was localized in a specific interval and no statistically significant coincidences occurred outside that interval. The slope of the

SI "triangle" is in good agreement with what was expected, meaning the neuron spikes synchronized with MNS timings were confined to a 10 s or smaller interval.

3.3. Multivariate synchrony index for intrinsic cardiac neurons

Figure 7 shows a 5,000-s portion of an experiment where 13 neurons were active. Total firing rate and MSI were calculated in time windows ranging from 10 to 180 s in duration and centered every 10 s. Looking at AF intervals delimited by vertical dashed lines, we notice that some neurons started firing during AF episodes, which contributed to increase total firing rate (Fig. 7B) and interestingly resulted in an increase in MSI (Fig. 7C).

Figure 8 displays a density plot representing the relation between MSI and the total firing rate for 10 dogs, where each point included in the density calculation corresponds to the MSI and firing rate data of a time window. Only data from windows where MSI was statistically significant ($p < 0.01$) were used. The plot shows that in most windows, $MSI < 0.2$ and that higher synchrony values occurred less frequently and were associated with low (< 1 Hz) firing rates. There is no data points near $MSI = 0$ because it would require a lot of data to identify a low but statistically significant value of MSI. There was no clear correlation between MSI and firing rate suggesting that the MSI provides additional information about intrinsic cardiac neurons that is independent from firing rate analysis.

Based on Eq. (16), it is possible to estimate an upper bound for MSI (assuming there are only two neurons) as a function of the total firing rate and the lowest (minimal) firing rate of the two neurons

$$MSI \leq 2\ f_{min}/f_{tot}\ . \tag{17}$$

Assuming $f_{min} = 0.5$ Hz, Eq. (17) is displayed as dashed line on Fig. 8, to which our data complies satisfactorily. The theoretical curve merely highlights the fact that a maximal MSI is only attainable when two spike trains are characterized by the same frequency (0.5 Hz in this case).

4. Discussion

The analysis of intrinsic cardiac neuron activity, a very recent field of research, has created new challenges. The relatively small density of neurons in ganglionated plexi, low firing rates, non-stationarity, the difficulty to obtain consistent response following repeated stimuli (average evoked response), and the interactions with and the multiple inputs from the cardiovascular and pulmonary systems require the development of dedicated tools different from what is known to work best for neuronal recordings in the brain.

In this article, we introduced a multivariate synchrony index (MSI) to provide a mean of characterizing synchrony in an ensemble of cardiac neurons with a single

symmetric measure that can be evaluated in a very large number of sliding windows over whole multiple-hour experiments. This index is structured as a sum of weighted SIs so that neurons with very low firing rates have a small contribution to the overall MSI, thus preventing possible neuron identification errors from introducing a large bias in the MSI. Each term of the sum involves the SI between a neuron and the combined time series of all other neurons, which increases the number of random coincidences in each SI contributing to MSI. On the other hand, the MSI may reveal global information about an ensemble of neurons that remains hidden when synchrony is evaluated pairwise. Note that the computational complexity of MSI is proportional to the number of neurons, while pairwise synchrony analysis depends on its square.

Cardiac neurons exhibit non-stationary activity, possibly switching between periods of high and low activity. These transitions may be triggered or modulated by external stimuli, the sympathetic or parasympathetic tone, changes in cardiovascular indices or cardiac rhythms such as the occurrence of arrhythmias. Neuron synchrony may also vary independently of firing rate, as suggested by Fig. 8. The identification of periods of interest (where significant changes in synchrony or firing rate are observed) is a critical task that may be time consuming when multiple hours of signal have to be examined. Automated analysis in sliding time windows of varying duration is a possible solution to that problem. However, most synchrony measures require explicit generation of surrogate data to assess statistical significance of synchrony so their application to 10^4–10^5 windows would become excessively computationally expensive. We extended Agmon's method to enable near real-time computation of synchrony in sliding windows over hours of data at about 10-s resolution.

We proposed a two-dimensional scale-time representation of the firing rate and synchrony in sliding time windows (e.g. Figs. 2 and 3). This representation is similar to spectrograms used in time-frequency analysis and greatly facilitates the exploration of the data set. In each window, the same weight was given to all the spikes. A smooth window function (such as Hamming window) could have been used in order to limit boundary effects. The cost of applying a window function would be to prevent the use of Eq. (15) and thus to considerably slow down computations. Consequently, the windowed approach might be used in a second stage after periods of interest have been identified.

Our approach was validated on synthetic time series, demonstrating its ability to independently assess firing rate and synchrony. For that purpose, we modified and extended Agmon's approach for synthetic signal generation to ensure an exact control of the SI and MSI. The method is however still limited to positive synchrony between a pair of neurons. The constraints involved in the simultaneous generation of more than two time series with given MSI remain unknown. The results on synthetic time series illustrated how to interpret experimental scale-time plots, notably in the case of abrupt transitions which are associated with a triangular pattern in the diagram (with characteristic slope of ± 2).

Applications of the scale-time representation of synchrony and firing rates were

illustrated using dog experiments. Examples of time-dependent synchrony between a neuron and left ventricular pressure (Fig. 4), respiration (Fig. 5) and external stimulation (Fig. 6), and time-dependent multivariate synchrony of a group of neurons (Fig. 7) were shown. These examples are not necessarily representative of the recorded neuron population. Indeed, many of them do not respond to cardiovascular, mechanical or respiratory inputs. The tools developed here are intended to identify those who respond synchronously and to test whether this synchrony is statistically significant and maintained over time. This methodology could be used to study in deeper details the interplay between the vulnerability to neurogenic atrial fibrillation and the synchrony of cardiac neurons.

Acknowledgments

This work was supported by the Natural Sciences and Engineering Research Council of Canada (V.J.), by the Fonds de Recherche du Québec – Santé (V.J.) and by NIH grant HL71830 (J.L.A.).

References

Agmon A 2012 A novel, jitter-based method for detecting and measuring spike synchrony and quantifying temporal firing precision *Neural Syst Circuits* **2**(1) 5.

Albo Z, Di Prisco G V, Chen Y, Rangarajan G, Truccolo W, Feng J, Vertes R P and Ding M 2004 Is partial coherence a viable technique for identifying generators of neural oscillations? *Biol Cybern* **90** 318–26.

Allefeld C and Kurths J 2004 An approach to multivariate phase synchronization analysis and its application to event-related potentials *Int J Bif Chaos* **14** 417–426.

Ardell J L 2004 *in* J. A Armour and J. L Ardell, eds, 'Basic and Clinical Neurocardiology' Oxford University Press New York.

Armour J A 2007 The little brain on the heart *Cleve Clin J Med* **74 Suppl 1** S48–51.

Armour J A 2008 Potential clinical relevance of the 'little brain' on the mammalian heart *Exp Physiol* **93**(2) 165–76.

Armour J A, Huang M H, Pelleg A and Sylven C 1994 Responsiveness of in situ canine nodose ganglion afferent neurones to epicardial mechanical or chemical stimuli *Cardiovasc Res* **28**(8) 1218–25.

Armour J A and Kember G C 2004 *in* J. A Armour and J. L Ardell, eds, 'Basic and Clinical Neurocardiology' Oxford University Press New York.

Ba D, Temereanca S and Brown E N 2014 Algorithms for the analysis of ensemble neural spiking activity using simultaneous-event multivariate point-process models *Front Comput Neurosci* **8**.

Baccala L A and Sameshima K 2006 Comments on "is partial coherence a viable technique for identifying generators of neural oscillations?": Why the term "Gersch causality" is inappropriate: common neural structure inference pitfalls *Biol Cybern* **95** 135–41.

Beaumont E, Salavatian S, Southerland E M, Vinet A, Jacquemet V, Armour J A and Ardell J L 2013 Network interactions within the canine intrinsic cardiac nervous system: implications for reflex control of regional cardiac function *J Physiol* **591**(Pt 18) 4515–33.

Gersch W and Goddard G 1970 Epileptic focus location: spectral analysis method *Science* **169** 701–2.

Hunter J, Milton J, Thomas P and Cowan J 1998 Resonance effect for neural spike time reliability *J Neurophysiol* **80** 1427–38.

Kaminski M J and Blinowska K J 1991 A new method of the description of the information flow in the brain structures *Biol Cybern* **65** 203–10.

Kreuz T, Chicharro D, Andrzejak R, Haas J and Abarbanel H 2009 Measuring multiple spike train synchrony *J Neurosci Methods* **183** 287–99.

Kreuz T, Chicharro D, Houghton C, Andrzejak R G and Mormann F 2013 Monitoring spike train synchrony *J Neurophysiol* **109** 1457–72.

Lindsey B G and Gerstein G L 2006 Two enhancements of the gravity algorithm for multiple spike train analysis *J Neurosci Methods* **150** 116–27.

Longpré J P, Salavatian S, Beaumont E, Armour J, Ardell J and Jacquemet V 2014 Measure of synchrony in the activity of intrinsic cardiac neurons *Physiol Meas* **35**(4) 549–66.

Pereda E, Quiroga R Q and Bhattacharya J 2005 Nonlinear multivariate analysis of neurophysiological signals *Prog Neurobiol* **77**(1-2) 1–37.

Tiesinga P 2004 Chaos-induced modulation of reliability boosts output firing rate in downstream cortical areas *Phys Rev E Stat Nonlin Soft Matter Phys* **69** 031912.

Figure legends

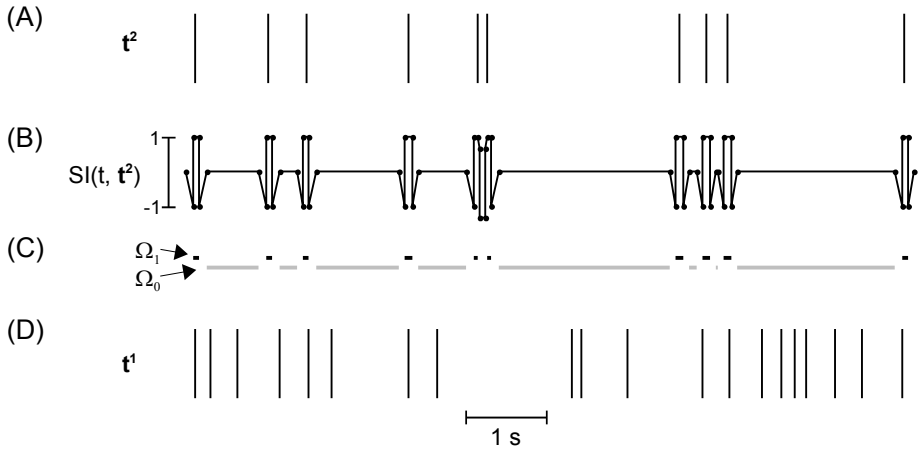

Figure 1. Two synthetic time series characterized by a chosen synchrony index of 0.3. (A) Target time series generated as realization of a Poisson process with a refractory period of $2\tau_s$. (B) Synchrony index as a function of time with respect to a reference spike added at time t. (C) The intervals where $SI(t, \mathbf{t}^2) = 1$ and $SI(t, \mathbf{t}^2) = 0$ are represented by the sets Ω_1 and Ω_0, respectively. (D) Spikes are placed in the sets Ω_1 and Ω_0 in order to get the desired $SI(\mathbf{t}^1, \mathbf{t}^2)$ value.

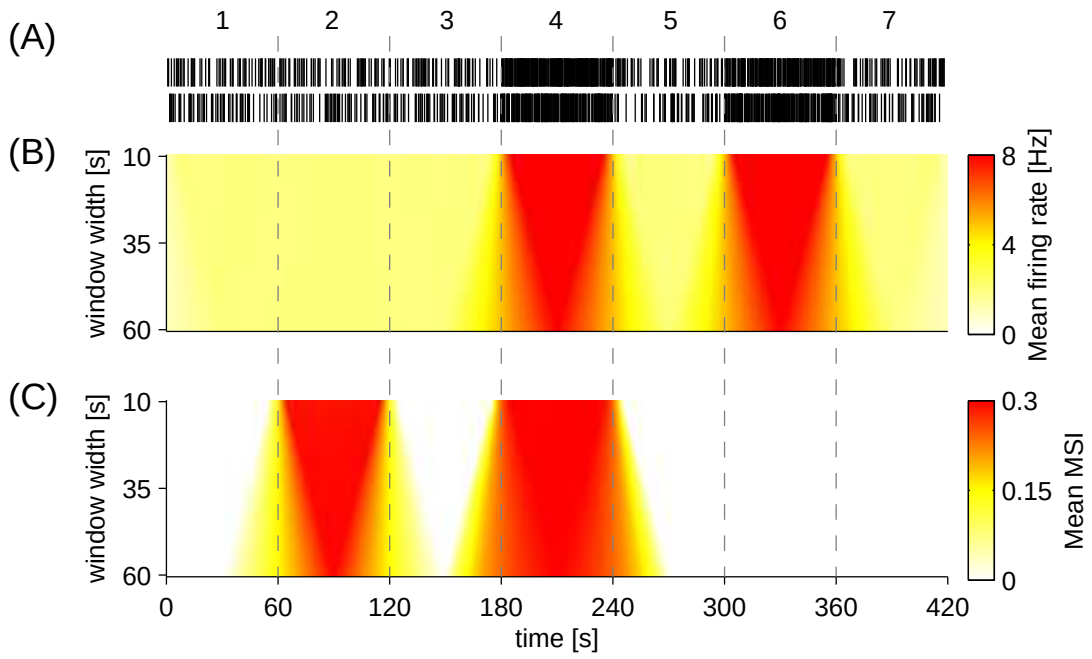

Figure 2. Mean firing rate and mean MSI from 5,000 realizations of two synthetic time series. Sliding windows used for calculation are between 10 and 60 s in duration at 1-s resolution. (A) An example realization of two synthetic time series with variable MSI and firing rate. In intervals 2 and 4, spikes were placed to get $SI = 0.3$. (B) Mean total firing rate from 5,000 realizations of the time series. (C) Mean MSI.

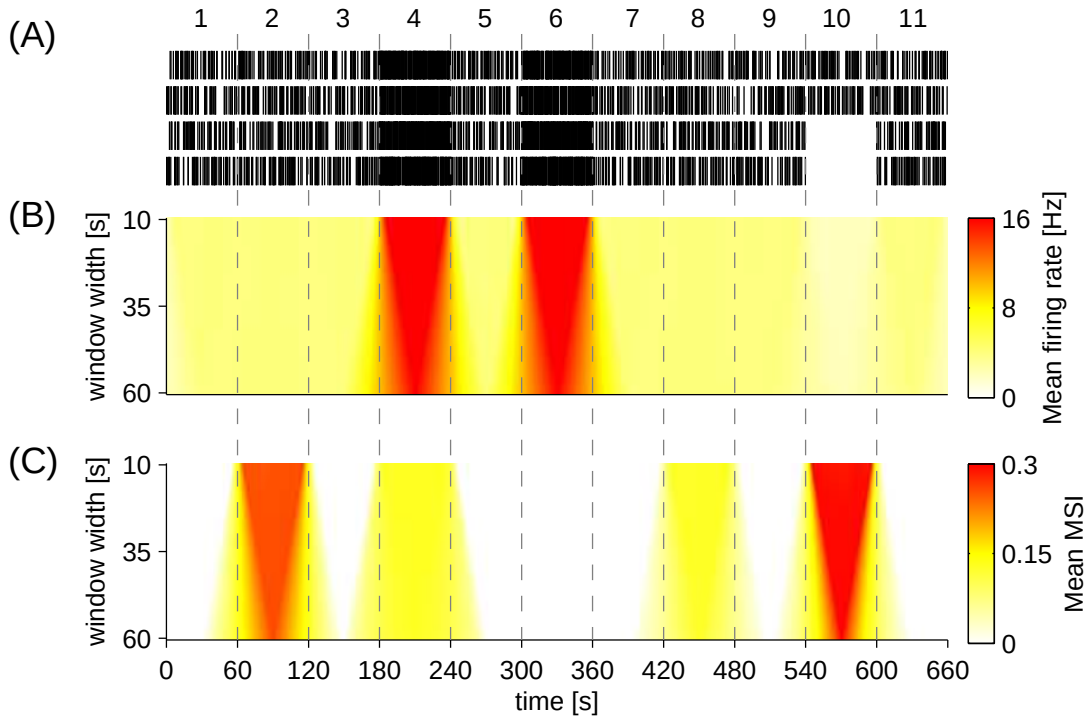

Figure 3. Mean firing rate and mean MSI from 5,000 realizations of four synthetic time series are calculated in sliding windows between 10 and 60 s in duration at 1-s resolution. (A) A random realization of four synthetic time series. Firing rate of each time series was set to 4 Hz in intervals 4 and 6, and to 1 Hz in all other intervals. SI of paired times series (two pairs) was set to 0.3 in intervals 2, 4, 8 and 10 (only one pair). (B) Mean total firing rate from 5,000 realizations of the time series. (C) Mean MSI.

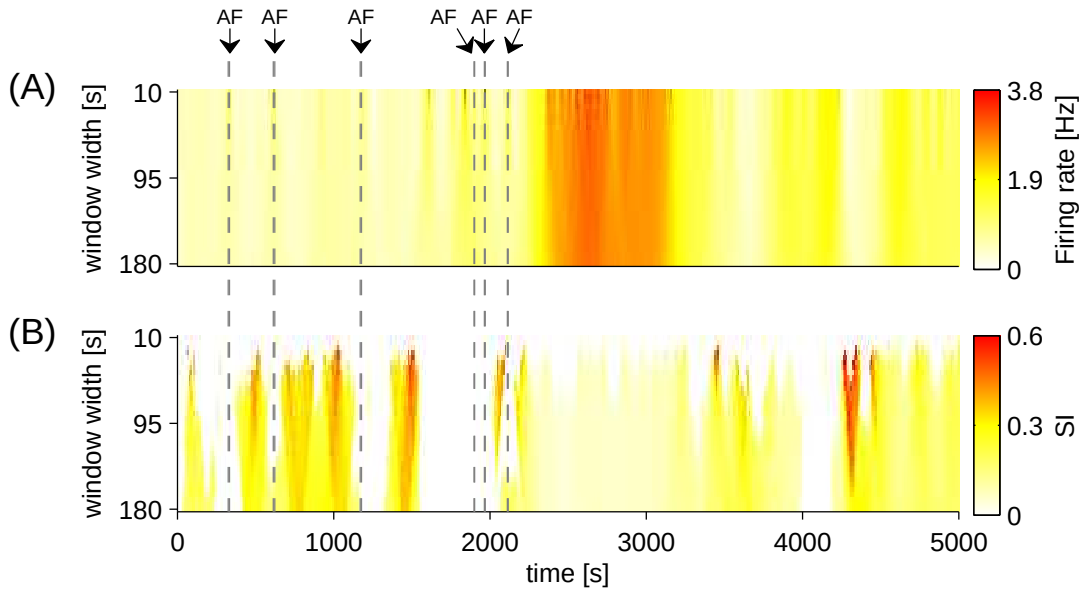

Figure 4. *SI* between left ventricular pressure (LVP) and the spikes of a neuron calculated in sliding windows between 10 and 180 s in duration at 10-s resolution. Intervals where atrial fibrillation (AF) episodes take place are indicated by arrows. Duration of AF episodes ranges from 5 to 20 s. (A) Firing rate of the neuron in time windows. (B) *SI* between neuronal spikes and LVP peaks. Neuronal spike train is considered the "reference" neuron in the computation of *SI*.

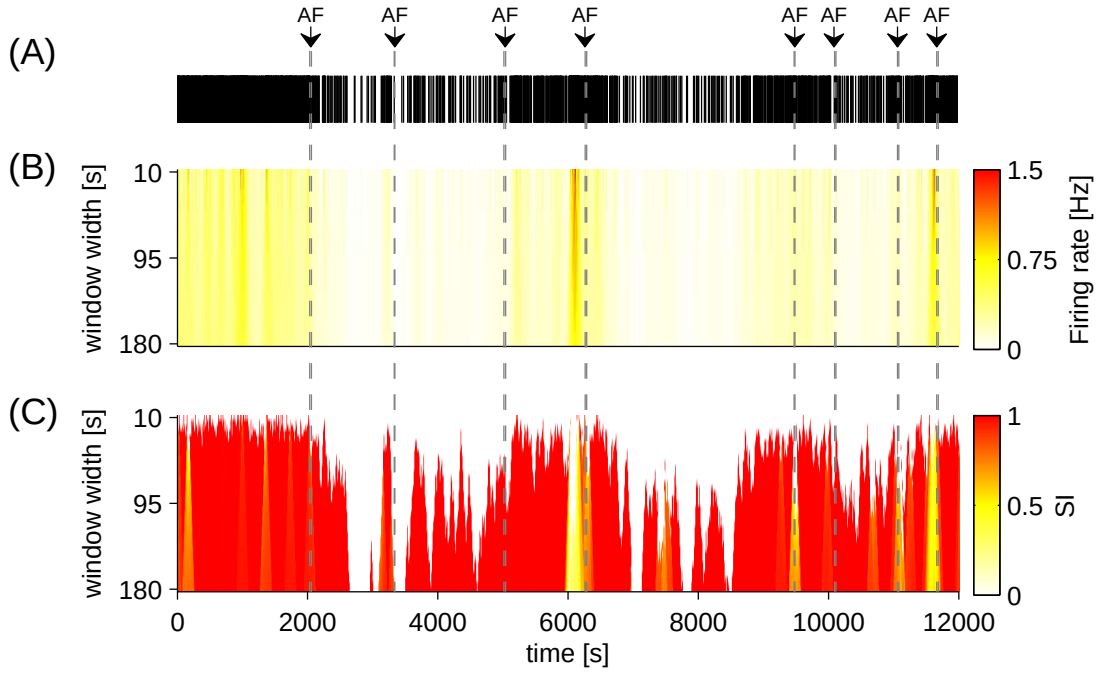

Figure 5. *SI* between respiration peaks and the spikes of a neuron calculated in sliding windows between 10 and 180 s in duration at 10-s resolution. Intervals where atrial fibrillation (AF) episodes take place are indicated by arrows. (A) Neuronal time series from a 12,000 s segment of an experiment. (B) Firing rate of the neuron calculated in sliding windows. (C) *SI* between spikes of the neuron and the repiration peaks, with the neuronal spike train acting as the "reference" neuron.

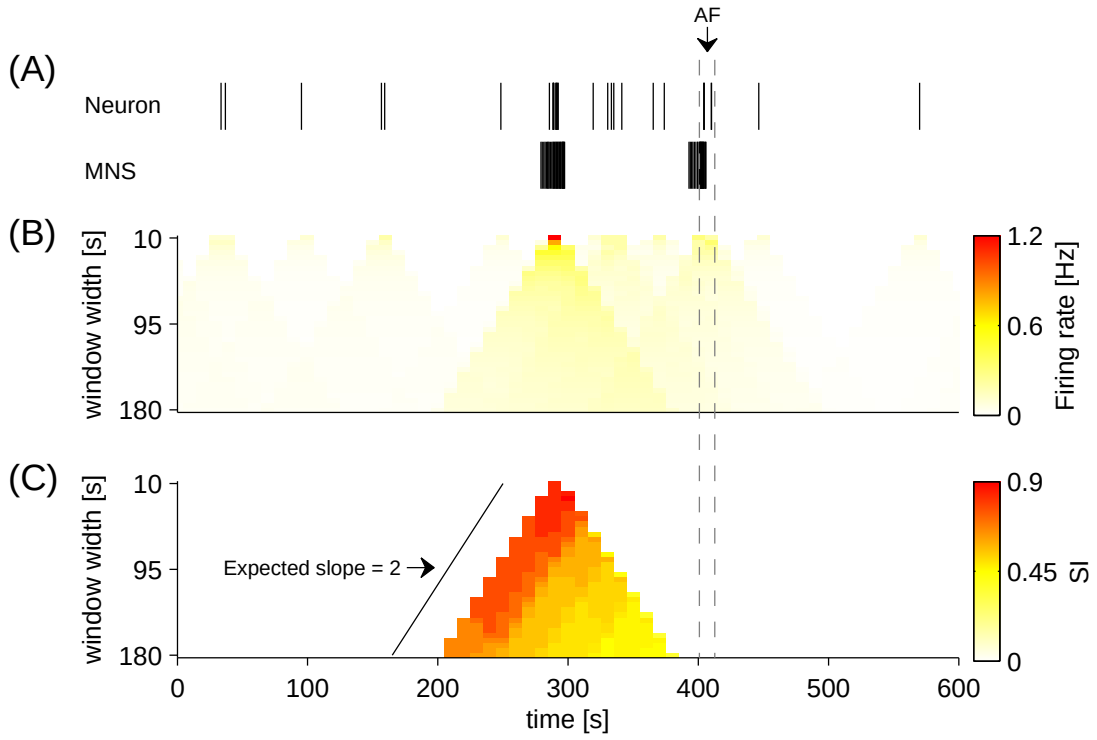

Figure 6. *SI* between MNS times and the spikes of a neuron calculated in sliding windows between 10 and 180 s in duration at 10-s resolution. An interval where an atrial fibrillation (AF) episode takes place is shown. (A) Neuronal spikes and MNS times from a 600 s segment of an experiment. (B) Firing rate of the neuron calculated in sliding windows. (C) *SI* between the neuron and MNS in time windows with the neuronal spike train taken as the "reference" neuron. A "triangle" of windows with a slope of 2 is expected when all significant coincidences occur only in a given interval (10 s in this case).

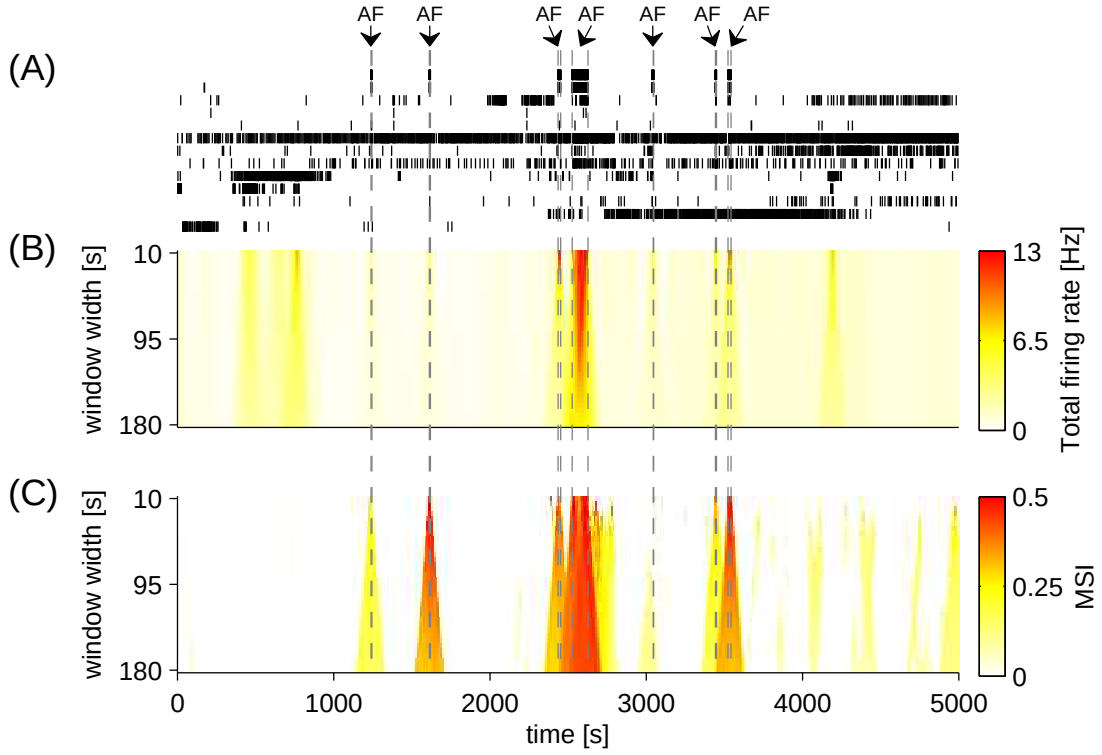

Figure 7. Neuronal time series with total firing rate and MSI calculated in sliding windows between 10 and 180 s in duration at 10-s resolution. Intervals where atrial fibrillation (AF) episodes occur are indicated by arrows. (A) Neuronal time series from a 5,000 s interval of an experiment. (B) Total firing rate calculated in sliding windows. (C) MSI in time windows.

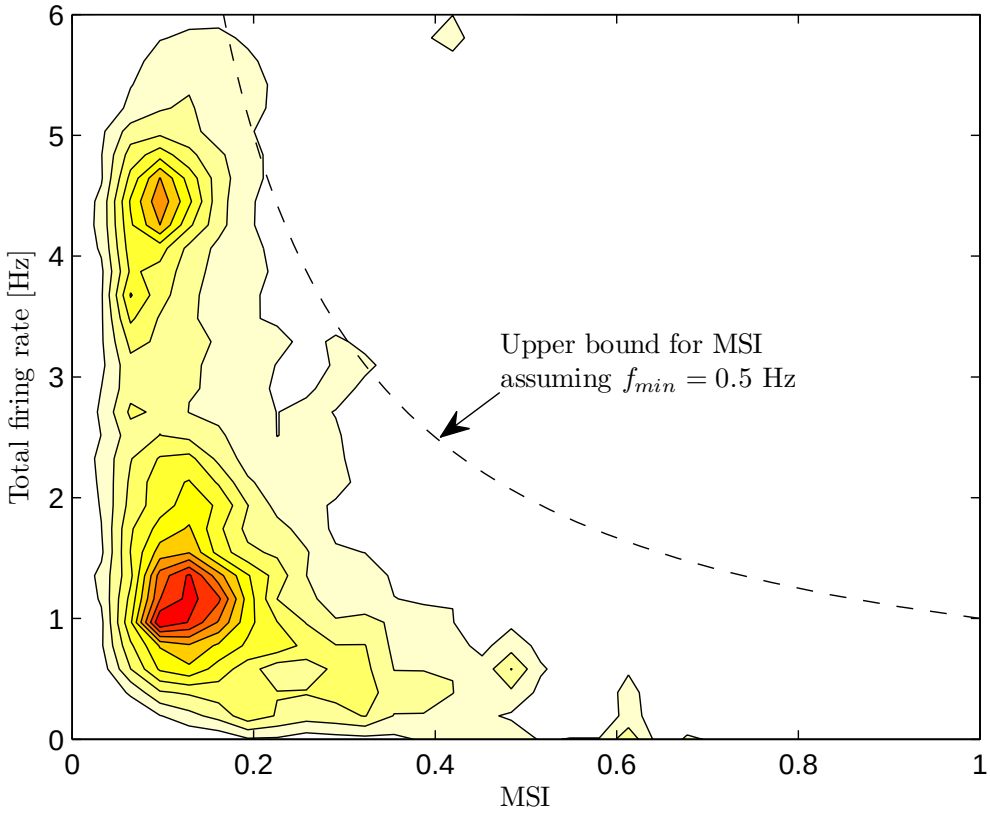

Figure 8. Density plot illustrating the relation between MSI and total firing rate calculated in sliding windows for all dogs. Only data from windows where MSI was statistically significant ($p < 0.01$) was used. Density is color-coded with white for low values ($= 0$) and red for high values. The dashed line refers to the upper bound for MSI calculated using $2\ f_{min}/f_{tot}$ where f_{tot} is the total firing rate and $f_{min} = 0.5$ Hz.